Published in final edited form as:
AIDS. 2012 November 13; 26(17): 2135–2144. doi:10.1097/QAD.0b013e328357f5ad.

Long-acting NanoART Elicits Potent Antiretroviral and Neuroprotective Responses in HIV-1 Infected Humanized Mice

Prasanta K. Dash[1], **Howard E. Gendelman**[1], **Upal Roy**[1], **Shantanu Balkundi**[1], **Yazen Alnouti**[1], **R. Lee Mosley**[1], **Harris A. Gelbard**[3], **JoEllyn McMillan**[1], **Santhi Gorantla**[1], and **Larisa Y. Poluektova**[1]

[1]Center for Neurodegenerative Disorders and Department of Pharmacology and Experimental Neuroscience, College of Medicine, University of Nebraska Medical Center, Omaha, NE, USA

[2]Department of Pharmaceutical Sciences, College of Pharmacy, University of Nebraska Medical Center, Omaha, NE, USA

[3]Center for Neural Development and Disease, College of Medicine, University of Rochester School of Medicine and Dentistry, Rochester, NY, USA

Abstract

Objectives—Long-acting nanoformulated antiretroviral therapy (nanoART) with improved pharmacokinetics, biodistribution and limited systemic toxicities will likely improve drug compliance and access to viral reservoirs.

Design—Atazanvir and ritonavir crystalline nanoART were formulated in a poloxamer-188 excipient by high-pressure homogenization. These formulations were evaluated for antiretroviral and neuroprotective activities in humanized NOD/*scid*-IL-2Rg$_c^{null}$ (NSG) mice.

Methods—NanoART-treated NSG mice were evaluated for drug biodistribution, pharmacodynamics and nanotoxicology. CD34$^+$ human hematopoietic stem cells were transplantation at birth in NSG mice. The mice were infected with HIV-1$_{ADA}$ at 5 months of age and 8 weeks later, infected animals were treated with weekly subcutaneous injections of nanoformulated ATV and RTV. Peripheral viral load, CD4$^+$ T cell count, lymphoid tissue and brain pathology were evaluated.

*Correspondence and reprint requests to: Howard E. Gendelman, MD, Department of Pharmacology and Experimental Neuroscience, 985880 Nebraska Medical Center, Omaha, NE 68198-5880, Phone: 402 559 8920, FAX: 402 559 3744, hegendel@unmc.edu.
HEG and LP contributed equally to this work.

The author reports no conflicts of interest.

Authorship contributions

PD performed the experiments and data analyses and wrote the first draft of the manuscript; HEG designed the experiments, interpreted and organized the data, wrote the paper and trouble shot the validation experiments; UR performed the drug delivery drug administration, analyzed drug levels and toxicity profiles, SB made the formulations and trouble shot their quality control measures, YA was responsible for the performance and interpretation of the UPLC assays used in the pharmacokinetic tests; RLM performed the statistical assays used in study and assisted in writing of the manuscript; HAG was responsible for the design and interpretation of the nervous system evaluations and testing before, during and following cessation of antiretroviral therapies; JM provided all the in vitro support for the quality control of the nanoformulations and designed and interpreted the toxicology data including renal, liver and metabolic functions as well as providing oversight for drug level analyses measures; SG performed and interpreted the flow cytometry data on T cells and T cell subsets; LP worked together with HEG on the overall experimental design and quality control and specifically for the virologic assessments and in both writing the paper and in coordinating the figures.

Results—NanoART treatments by 6 once a week injections reduced viral loads >1000 fold and protected $CD4^+$ T cell populations. This paralleled high ART levels in liver, spleen and blood that were in or around the human minimal effective dose concentration without notable toxicities. Importantly, examination of infected brain subregions showed that nanoART elicited neuroprotective responses with detectable increases in microtubule-associated protein-2, synaptophysin and neurofilament expression when compared to untreated virus-infected animals. Therapeutic interruptions produced profound viral rebounds.

Conclusions—Long-acting nanoART has translational potential with sustained and targeted efficacy and with limited systemic toxicities. Such success in drug delivery and distribution could improve drug adherence and reduce viral resistance in infected people.

Keywords

Human immunodeficiency virus type one; HIV-associated neurocognitive disorders; Humanized mice; Nanoformulated antiretroviral therapy; Drug biodistribution; Central nervous system

INTRODUCTION

Drug regimen adherence and long-term systemic toxicities are notable risk factors for safety and efficacy of lifelong antiretroviral therapy (ART)[1]. The establishment of ART depots would circumvent this risk by requiring less frequent drug administrations[2]. Others and we developed manufacturing techniques to package antiretroviral drugs into long-acting nanoformulations for sustained drug release[3–5]. While prior clinical studies support the idea that viral suppression could be achieved with a simplified regimen of protease inhibitors atazanvir (ATV) and ritonavir (RTV)[6, 7], none have created long-acting antiretroviral formulations nor correlated immune outcomes with drug distribution to tissue viral reservoirs. Surprisingly, no previous studies correlated end organ or HIV-affected disease outcomes with ART. Thus, we chose to formulate ATV and RTV in order to facilitate drug delivery to maintain viral suppression. Both are safe, well tolerated and efficacious in suppressing viral replication. Therefore, we prepared ATV and RTV ART nanoformulations (nanoART) using a Food and Drug Administration-approved excipient (poloxamer 188; P188) by homogenization procedures developed in our laboratories[8]. Drug encapsulation through such methods results in high ART load per volume ratios with optimal shape and sizes enabling rapid uptake and sustained drug release[3, 5, 9, 10].

ART efficacy and toxicity measures can readily be performed in HIV-infected NOD/*scidIL-2R*g_c^{null} (NSG) mice transplanted with human hematopoietic $CD34^+$ stem cells (HSC) (hu-NSG mice). This new generation of mice, developed in others and our laboratories, permits an extended engraftment of a human immune system and enables a unique platform for testing long-acting ART[11–13]. Due to longer graft stability and extended end-point evaluations, the model represents a noted advance for HIV-1 therapeutic testing paradigms[14, 15].

NanoART efficacy was assessed in HIV-1-infected hu-NSG mice injected subcutaneously (s.c.) at weekly dosing intervals. Treatments led to robust tissue drug depots within the reticuloendothelial system and ART concentrations in blood at therapeutic levels. We also

demonstrated nanoART maintenance of synaptodendritic morphology, a key pathologic substrate for neurocognitive impairment. Systemic toxicities were limited. Modest changes in serum albumin and blood urea nitrogen were observed, but only secondary to co-morbid infection and not to nanoART. All together, the consistently robust pharmacodynamic changes in immune restoration and antiretroviral responses strongly support the potential of nanoART for human use.

MATERIALS AND METHODS

Mice

NSG mice (The Jackson Laboratories, stock number 005557) were obtained from the established breeding colony and housed under pathogen-free conditions in accordance with ethical guidelines for care of laboratory animals at the National Institutes of Health and the University of Nebraska Medical Center.

NanoART manufacture and in vitro uptake/release characterization

Free-base RTV was purchased from Shengda Pharmaceutical Co., Zhejiang, China. ATV-sulfate was procured from Gyma Laboratories of America Inc., Westbury, NY. Nanoformulations using the excipient poloxamer-188 (P188; Sigma-Aldrich, St. Louis, MO) and free base drug were prepared by high-pressure homogenization as described[8, 9]. Drug content was determined by reverse phase high performance liquid chromatography (RP-HPLC)[10] and by ultra performance liquid chromatography tandem mass spectrometry (UPLC-MS/MS) using a Waters ACQUITY UPLC (Waters, Milford, MA) coupled to an applied Biosystems 4000 Q TRAP quadruple linear ion trap hybrid mass spectrometer (Applied Biosystems/MDS Sciex, Foster City, CA)[16]. Lyophilized particles were resuspended in saline prior to animal injections. For scanning electron microscopy (SEM), 10 μl of nanosuspension were diluted in 1.5 ml of 0.2 μm filtered distilled water and prepared for morphologic examination using a Hitachi S4700 Field-Emission Scanning Electron Microscope (Hitachi High Technologies America, Inc., Schaumburg, IL) (Figure 1A). *In vitro* uptake and release of ATV and RTV was determined in human monocyte-derived macrophages (MDM)[5]. Human monocytes obtained by elutriation were cultured for seven days in the presence of macrophage colony stimulating factor (MCSF), a generous gift by Pfizer Pharmaceuticals, Cambridge, MA. MDM and culture media were collected from cells treated with 100 mM nanoART and extracted using methanol for drug level determinations (Figure 1B) as previously described[10].

Drug biodistribution assessments

Ten week-old NSG mice were administered nanoART s.c. at six weekly doses of 250 mg/kg of ATV and RTV (total n = 45, 5 mice/week). Five mice were sacrificed 3 weeks after drug cessation. The drug concentrations found in sera of NSG mice corresponded to a human dose 20.3 mg/kg based upon an interspecies scaling factor of 12.3[14]. Animals were sacrificed weekly and up to 3 weeks following the last dose for determination of drug levels in serum, liver and spleen.

Generation, selection, infection and treatment of humanized mice

$CD34^+$ HSC were obtained from fetal liver (University of Washington, Laboratory of Developmental Biology supported by NIH Award Number 5R24HD000836) or human cord blood (Department of Gynecology and Obstetrics, UNMC) using magnetic beads CD34+ selection kit (Miltenyi Biotec Inc., Auburn, CA). Animals were transplanted as previously described[13]. Human pan-CD45, CD3, CD4, CD8, CD14, and CD19 markers were assayed as a six-color combination (BD Pharmingen, San Diego, CA) using a fluorescence-activated cell sorting (FACS) Diva (BD Immunocytometry Systems, Mountain View, CA) system. The percentages of $CD4^+$ and $CD8^+$ cells were obtained from the gate set on human CD3+ cells. Animals were infected with HIV-1_{ADA} (i.p.) at a dose of 10^4 $TCID_{50}$/mouse. The levels of viral RNA copies/ml in plasma were monitored by automated COBAS Amplicor System v1.5 (Roche Molecular Diagnostics, Basel, Switzerland) as described[17]. NanoART was injected in HIV-1 infected and uninfected (control) animals of the same age (n = 5). NanoART was discontinued after six injections and animals were evaluated for an additional three weeks. At the study termination, spleen, thymus, lymph nodes, liver, lungs, kidney and brain tissues were collected for cell and viral tests[17].

Serum biochemistry and tissue histopathology

Serum chemistry profiles were achieved using a VetScan comprehensive diagnostic profile disc interfaced with a VetScan VS-2 instrument (Abaxis Inc., Union City, CA). For immunohistochemical analysis, tissues were fixed with 4% paraformaldehyde and embedded in paraffin. Five-micron thick sections were immunostained for CD45LCA (Dako, Carpinteria, CA 1:200), HLA-DR (clone CR3/43, 1:100) and HIV-1 p24 (1:10)[13, 18]. Images were obtained with a Nuance EX camera fixed to a Nikon Eclipse E800 using Nuance software (Cambridge Research & Instrumentation, Woburn, MA).

Immunofluorescence labeling, multispectral imaging and image analyses

Slide specimens (5μm thick) of paraffin-embedded mouse brains were selected. Brain sections were treated with different paired combinations of primary mouse monoclonal antibodies to 200 kDa and 68 kDa neurofilaments (NF) (clone 2F11; 1:200; Dako) and synaptophysin (SYN) (1:1000; Novus Biologicals, Littleton, CO) and rabbit polyclonal antibodies to MAP2 and GFAP. Primary antibodies were labeled with secondary anti-mouse and anti-rabbit antibodies conjugated to the fluorescent probes Alexa Fluor 488 and Alexa Fluor 594, and nuclei were labeled with 4′, 6-diamidino-2-phenylindole (DAPI). Slides were coverslipped with ProLong Gold anti-fade reagent (Invitrogen, Carlsbad, CA), allowed to dry for 24 h at room temperature, and then stored at -20°C for future use. Images were captured at wavelengths encompassing the emission spectra of the probes, with a 20× and 40× objectives. The fluorescence emission of each probe and autofluorescence of the tissue samples were analyzed and quantitated by multispectral imaging/image analysis as described[17].

Statistical analysis

Statistics were summarized using medians and means. The values of cell surface markers CD45, CD4, CD8, CD14 and CD3 were averaged from all the mice. Statistical comparisons

were assessed between two groups using a Mann-Whitney U-test and Statistical Package for the Social Sciences. Differences were considered significant at $P < 0.05$.

RESULTS

NanoART manufacture, characterization and biodistribution

ATV and RTV nanoformulations were characterized by morphology and physical properties. ATV nanoformulations appeared as long slender rods, while RTV formulations were rectangular by scanning electron microscopy (Fig. 1A). *In vitro* uptake of ATV and RTV nanoformulations by human monocyte-derived macrophages (MDM) reached 8.1 ± 0.4 (± SEM) and 16.2 ± 0.5 mg/10^6 cells, respectively. Drug release peaked at day 1 and was sustained until day 10 for RTV. For ATV the peak drug release was on day 5 and reduced to levels of ~2 mg/ml on days 10 to 15 (Fig. 1B). Uptake and long-term release of nanoformulated drugs suggested that macrophages provide therapeutically useful reservoirs of drug and could serve as nanoparticle depots for long-term release.

To assess nanoART *in vivo* biodistribution, nanoformulations of ATV and RTV at 1:1 ratios were administered to NSG mice at weekly intervals for 6 weeks. These experiments were performed prior to evaluation of antiretroviral responses to ensure that the correct drug concentrations and dosing intervals were used. The timing of the drug injections is shown by red arrows (Fig. 1C&D). The ratios of ATV and RTV employed were based on previously optimized data sets [10]. ATV serum levels reached a peak median concentration of 186 ng/ml by week 6 (Fig. 1C), a level above the minimum effective plasma concentration of 150 ng/ml[19]. Peak RTV serum levels of 213 ng/ml were achieved by week 5. NanoART cessation for three weeks led to a drop of serum drug levels to 45–80 ng/ml (week 8). Liver and spleen drug levels however were relatively constant from 1,000 to over 10,000 ng/ml for both drugs (Fig. 1D).

In HIV-1 infected humanized mice, after 2 weekly nanoART s.c. injections, mean ATV and RTV levels were 552 and 233 ng/ml in serum, 2407 and 2370 ng/g of tissue in liver (Table 1), 3065 and 798 ng/g in spleen, and 237 and 191 ng/g in lungs. After 3 weeks of drug interruption in HIV-1 infected mice group, liver drug median ATV and RTV concentrations were 1089 ng/g (364 – 5663) and 376 ng/g (144 – 515) of tissue weight (Table 1). Median serum concentrations were 227 ng/ml (128 – 237) for ATV and 40 ng/g (32 – 95) for RTV. Notably, there was a significant reduction of RTV compared to ATV serum concentrations in 9 month-old compared to 10 week-old NSG mice thereby reflecting age-dependent metabolism of protease inhibitors[20]. Control (uninfected) humanized mice of the same age and sex (females) treated with nanoART for 6 weeks followed by 3 weeks of drug interruption showed ATV and RTV levels in sera and liver at a median of 367 and 54 ng/ml and 1816 and 690 ng/g of tissue, respectively (data not shown). Significant differences in serum ATV and RTV concentrations were observed in human cell reconstituted mice as compared to mice that were not reconstituted ($P = 0.008$, Mann-Whitney U-test).

Antiretroviral responses of nanoART treated humanized mice

Hu-NSG mice were infected with HIV-1_{ADA} at 22 weeks of age (Fig. 2A). All mice selected for studies (n =18) retained circulating human $CD45^+$, $CD4^+$, $CD8^+$ T cells, $CD19^+$ B cells and $CD14^+$ monocytes and had stable human lymphoid grafts. This was demonstrated by fluorescence-activated cell sorting (FACS) testing of peripheral blood leukocytes, splenocytes and bone marrow cells (Supplemental digital content Table 1). The FACS gating strategy for human-specific hematopoietic cells in peripheral blood of hu-NSG mice is shown in Fig. 2B.

Antiviral activity was assessed following weekly 250 mg/kg nanoART injections administered to chronically HIV-infected hu-NSG mice on whom treatment was begun at 8 weeks post-infection (WPI) (Fig. 2A). In all ART naive virus-infected animals, viral infection was sustained with a median viral load (VL) of 1.63×10^5 copies/ml with one exception, where it was detected at 4 weeks after infection (3040 copies/ml) and remained below the detection limit (2500 copies/ml taking into consideration the limited mouse sample volumes available) for study evaluation. To assess nanoART efficacy, chronically HIV-1-infected hu-NSG mice were divided into untreated (control, $n = 6$) and treated (nanoART) groups ($n = 7$). Two HIV mice were sacrificed one week after two weekly nanoART injections. Animals were evaluated for levels of CD45 (Table 1) and total CD3, CD4, CD8 cell counts and VL in blood at 8 weeks after infection (Fig. 2B), and reductions in human $CD4^+$ T cells were observed. FACS analysis of the peripheral blood after 6 weekly nanoART injections (each injection is illustrated by a red arrow) showed a significant protection of human $CD3^+CD4^+$ T cells in treated versus control mice (Fig. 2C). After 4 nanoART injections, VL was reduced by 100 to 1000 fold and was at or below 2500 copies/ml, the limits of assay detection for analyzed samples (Fig. 2D). After 6 injections, therapy ended and animals were evaluated after an additional 3 weeks of therapeutic cessation. Virus rebound was observed in 4 of 5 animals (Fig. 2D, nanoART injection times are shown by red arrows). The highest VLs were in animals with the lowest plasma ATV concentrations in serum (Table 1). NanoART also prevented HIV-1 infection-induced increases of CD45+ and $CD8^+$ cell numbers in bone marrow, spleen and blood (Supplemental digital content Table 1).

Histopathological and immunohistochemical changes in infected and/or nanoART-treated animals are shown in Fig. 3. Lymph node sizes were reduced by up to 50% in HIV-1 infected mice compared to infected and nanoART-treated mice (Fig. 3A). Interestingly, the medullar regions of the lymph nodes in reconstituted animals were occupied by immature human B cells (Fig. 3A) shown by IgM staining. By three weeks after nanoART cessation, the lymphoid organs have an increased expression of HIV-1p24 positive cells (Fig. 3B). Equivalent numbers of human cells were in the liver and lung in both groups as shown by HLA-DR staining with readily identified HIV-1 $p24^+$ cells in untreated animals (Fig. 3C). Three treated animals with the lowest VL (217, 1930 and <2500 copies/ml) retained HIV-1 $p24^+$ infected cells in the lymph nodes (Fig. 3D).

Drug toxicity profiles for nanoART in HIV-infected mice

Reduction in animal weight was observed after the first nanoART injection regardless of infection with a median loss of 5.6% (ranged 15.5 ± 0.1%, *n*=12). Compared to initiation of nanoART treatment, HIV-infected mice regardless of the treatment regimen did not experience significant differences in weight loss (8% ± 3% and 7% ± 3%, respectively) (data not shown). The site of the drug injection showed visible drug depots under the skin without erythema or tissue injury. However, accumulation of mouse and human macrophages were readily observed around places of nanosuspension injections as shown by Iba-1 staining (Supplemental digital content Fig. 1). Serum chemistry profiles for treated and control animals evaluated at study end showed reduced serum albumin in infected control untreated animals not in treated group, and elevated blood urea nitrogen levels (Supplemental digital content Table 2). The changes in blood urea nitrogen (BUN) reflect co-morbid infections in some of the uninfected animals not toxicity.

NanoART protection of HIV-1 induced neural injury

To determine *in vivo* changes in brain architecture, neuronal and glial antigens were analyzed by multispectral fluorescence microscopy of replicate brain regions sampled at study termination. Cortical neurons of HIV infected animals showed decreased expression of microtubule associated protein 2 (MAP2+) dendrites; whereas, animals sacrificed one week after two nanoART injections showed significant ($P = 0.048$) increase in expression of MAP2+ dendrites with normal morphology (Fig. 4A). After the 3-week nanoART interruption, MAP2 expression was diminished; and neuronal architecture was irregular with wavy contours similar to untreated infected mice.

Synaptophysin (SYN) expression in cortical areas of controls or animals sacrificed one week after nanoART treatment was observed as diffusively punctate; whereas, SYN expression was irregularly shaped in both the infected and treatment interrupted group (Fig. 4A). Reduction of NF-positive fibers was observed in the cortex of animals with high VL (both infected and interrupted treatment group), compared to animals with undetectable viral load after one week of 2 nanoART treatments (Fig. 4B). The images captured using 20× objectives were converted to 12 bit grey scale images and used for quantification. The intensities of MAP2, SYN, neurofilaments (NF) and glial fibrillary acidic protein (GFAP) expression were quantitated as total area labeled (Supplemental digital content Fig. 2A&B). Animals that were either uninfected or HIV-1 infected and nanoART-treated showed normal brain morphology compared to HIV-infected mice. Increased NF expression was observed in both the cerebral cortex and whisker barrels in nanoART-treated infected mouse brains as compared of virus-infected controls (Fig. 4B). The most significant changes were observed in the MAP2 structure and expression in the cerebral cortex and whisker barrels of mice treated twice with nanoART and sacrificed after 7 days (Supplemental digital content Fig. 2A&B) compared to infected untreated group. We also observed a similar pattern of increase in expression in the quantitation of NF and SYN in the nanoART treated mice but not as pronounced as MAP2 (data not shown).

DISCUSSION

Drug-associated viral escape from immune surveillance, ART penetration into viral reservoirs and long-term toxicities are limitations of combination ART[21, 22]. We posit that each of these limitations can be overcome, in whole or in part, through the development of long-acting nanoART[23, 24]. We fully understand that enabling this process while requiring multidisciplinary approaches in polymer chemistry, cell biology, nanotoxicology, virology, immunology and animal modeling to successfully establish the therapeutic utility of nanoART in relevant animal model of chronic HIV-1 disease also requires patient acceptance of the principals. To this end, a recent clinical epidemiology study demonstrated significant patient support for the type of injectable long-acting nanoART used in this report compared against conventional drug therapy (Susan Swindells, personal communication).

The premise of such a drug delivery system resides in the fact that drugs stored in polymer excipients can be readily taken up and stored for extended time periods in tissue skin and macrophages depots. We have recently shown improved access of nanoART to viral CNS reservoirs[25] with only subtle immune activation of macrophages. In recent works performed in our laboratory we showed that 90% of the nanoART seen in liver after s.c. injection of rodents was in Kupffer cells (Upal Roy, unpublished data). This permits not only the establishment of a cellular depot of ART but also a means for long-term drug protection against metabolism and reduced systemic toxicities as would occur following oral administrations. Drug compartmentalization inside cells could influence natural immunity against the polymer. The potential of monocyte-macrophages to serve as “Trojan Horses” for nanoART delivery also facilitates drug delivery to specific sites of active viral infection and replication resulting in another boost to conventional therapeutic options. In screening studies, NSG mice were reconstituted with human peripheral blood lymphocytes then infected and nanoART treated. These animals showed improved biodistribution and drug activity. The single oral administration of native drugs 24h before infection was not effective, whereas a single subcutaneous administration of nanoART at an equal dose of 250mg/kg significantly reduced levels of infection and drug levels in serum and peripheral tissues sustained for 9 days[26].

The improved PK of selected nanoformulated protease inhibitors was observed in presented studies after multiple administrations. ATV serum levels were 114 – 162 ng/ml. This is coincident with the 50 percent inhibitory concentration (100 ng/ml) for the virus. At study end, the median values of ATV and RTV levels in the liver were higher than seen in lung and spleen. A differential pattern of drug concentrations in nanoART-treated mice can be attributed to age[27] and gender[28] influences on cytochrome P450 activity. The distinct metabolism between mice and humans needs to be considered when extrapolating drug concentrations for clinical use[14].

NanoART treatment resulted in the protection of human $CD4^+$ cells in the peripheral compartment and the reduction of viral load. As we have reported previously, chronic HIV-1 infection in humanized mice induced changes in neuronal morphology[29–31] and significant reduction of the expression of synaptic, dendritic and axonal proteins[17]. NanoART treatment when initiated eight weeks after infection and following only two

weekly injections was coincident with the restoration of neuronal antigen expression in treated HIV-infected animals. The protection of CD4+ cells and significant reduction of peripheral VL can be correlated to the reversal of damaged neuronal dendritic morphology. The damaged neuronal architecture seen in nanoART treated animals after treatment interruption demonstrated that the observed neuropathologic protection could be reversed and also correlated to increased VL. Another surprising observation was the presence of "therapeutic" ATV concentrations in blood during viral rebound. This finding certainly requires future investigation to clarify real ATV bioavailability and development of viral resistance.

NanoART treatment in chronically infected humanized mice failed to effectively suppress viral replication in the lymph nodes as detected by strong HIV-1 p24 expression and suggested the inability of ATV to effectively penetrate lymphoid tissues as described for virus-infected people given native drug[32]. However, treated animals have better preserved thymus structure with reduced numbers of human activated HLA-DR cells and lower presence of immature IgM (Fig. 3A) and IgG-negative B cells. Humanized mice do provide a platform for testing ART efficacy that mimics human disease. In these studies nanoART was effective in reducing ongoing HIV-1 replication.

The observed changes in the serum albumin level in infected untreated mice and elevated blood urea nitrogen as compared to the nanoART-treated group can be attributed to age[33], animal food and water intake as well as sporadic kidney infection. The relationship between these findings and viral infection is under current investigation[34]. These data, taken together, demonstrate nanoART efficacy patterns close to infected ART-treated humans.

Conclusion

Overall this study demonstrates improved drug carriage and ART release through nanoformulation and gives further support to the translation of nanoART to the clinic. Important targets for such developments are protease inhibitors (ATV/RTV), which can be used for maintenance therapy in ART-experienced patients[2, 6, 35].

Supplementary Material

Refer to Web version on PubMed Central for supplementary material.

Acknowledgments

The work was supported by the National Institutes of Health grants 1P01 DA028555, 2R01 NS034239, 2R37 NS36126, P01 NS31492, P20RR 15635, P30 MH062261, P01MH64570 (HAG) and P01 NS43985 and from a research grant from Baxter Healthcare. The authors thank Jaclyn Knibbe, Tanuja Gutti, Edward Makarov, Nathan Smith, Ram Veerubhotla, and Landon Ehlers for their expert technical assistance.

References

1. Volberding PA, Deeks SG. Antiretroviral therapy and management of HIV infection. Lancet. 2010; 376:49–62. [PubMed: 20609987]
2. Swindells S, Flexner C, Fletcher CV, Jacobson JM. The critical need for alternative antiretroviral formulations, and obstacles to their development. J Infect Dis. 2011; 204:669–674. [PubMed: 21788451]

3. Kadiu I, Nowacek A, McMillan J, Gendelman HE. Macrophage endocytic trafficking of antiretroviral nanoparticles. Nanomedicine (Lond). 2011; 6:975–994. [PubMed: 21417829]
4. Mallipeddi R, Rohan LC. Progress in antiretroviral drug delivery using nanotechnology. Int J Nanomedicine. 2010; 5:533–547. [PubMed: 20957115]
5. Nowacek AS, Miller RL, McMillan J, Kanmogne G, Kanmogne M, Mosley RL, et al. NanoART synthesis, characterization, uptake, release and toxicology for human monocyte-macrophage drug delivery. Nanomedicine (Lond). 2009; 4:903–917. [PubMed: 19958227]
6. Wilkin TJ, McKinnon JE, DiRienzo AG, Mollan K, Fletcher CV, Margolis DM, et al. Regimen simplification to atazanavir-ritonavir alone as maintenance antiretroviral therapy: final 48-week clinical and virologic outcomes. J Infect Dis. 2009; 199:866–871. [PubMed: 19191590]
7. Swindells S, DiRienzo AG, Wilkin T, Fletcher CV, Margolis DM, Thal GD, et al. Regimen simplification to atazanavir-ritonavir alone as maintenance antiretroviral therapy after sustained virologic suppression. JAMA. 2006; 296:806–814. [PubMed: 16905786]
8. Balkundi S, Nowacek AS, Veerubhotla RS, Chen H, Martinez-Skinner A, Roy U, et al. Comparative manufacture and cell-based delivery of antiretroviral nanoformulations. Int J Nanomedicine. 2011; 6:3393–3404. [PubMed: 22267924]
9. Balkundi S, Nowacek AS, Roy U, Martinez-Skinner A, McMillan J, Gendelman HE. Methods development for blood borne macrophage carriage of nanoformulated antiretroviral drugs. J Vis Exp. 2010
10. Nowacek AS, Balkundi S, McMillan J, Roy U, Martinez-Skinner A, Mosley RL, et al. Analyses of nanoformulated antiretroviral drug charge, size, shape and content for uptake, drug release and antiviral activities in human monocyte-derived macrophages. J Control Release. 2011; 150:204–211. [PubMed: 21108978]
11. Sato K, Koyanagi Y. The mouse is out of the bag: insights and perspectives on HIV-1-infected humanized mouse models. Exp Biol Med (Maywood). 2011; 236:977–985. [PubMed: 21750016]
12. Berges BK, Rowan MR. The utility of the new generation of humanized mice to study HIV-1 infection: transmission, prevention, pathogenesis, and treatment. Retrovirology. 2011; 8:65. [PubMed: 21835012]
13. Gorantla S, Sneller H, Walters L, Sharp JG, Pirruccello SJ, West JT, et al. Human immunodeficiency virus type 1 pathobiology studied in humanized BALB/c-Rag2−/−gammac−/− mice. J Virol. 2007; 81:2700–2712. [PubMed: 17182671]
14. Stoddart CA, Bales CA, Bare JC, Chkhenkeli G, Galkina SA, Kinkade AN, et al. Validation of the SCID-hu Thy/Liv mouse model with four classes of licensed antiretrovirals. PLoS One. 2007; 2:e655. [PubMed: 17668043]
15. Choudhary SK, Rezk NL, Ince WL, Cheema M, Zhang L, Su L, et al. Suppression of human immunodeficiency virus type 1 (HIV-1) viremia with reverse transcriptase and integrase inhibitors, CD4+ T-cell recovery, and viral rebound upon interruption of therapy in a new model for HIV treatment in the humanized Rag2−/−{gamma}c−/− mouse. J Virol. 2009; 83:8254–8258. [PubMed: 19494021]
16. Huang J, Gautam N, Bathena SP, Roy U, McMillan J, Gendelman HE, et al. UPLC-MS/MS quantification of nanoformulated ritonavir, indinavir, atazanavir, and efavirenz in mouse serum and tissues. J Chromatogr B Analyt Technol Biomed Life Sci. 2011; 879:2332–2338.
17. Dash PK, Gorantla S, Gendelman HE, Knibbe J, Casale GP, Makarov E, et al. Loss of neuronal integrity during progressive HIV-1 infection of humanized mice. J Neurosci. 2011; 31:3148–3157. [PubMed: 21368026]
18. Poluektova LY, Munn DH, Persidsky Y, Gendelman HE. Generation of cytotoxic T cells against virus-infected human brain macrophages in a murine model of HIV-1 encephalitis. J Immunol. 2002; 168:3941–3949. [PubMed: 11937550]
19. Boffito M, Jackson A, Amara A, Back D, Khoo S, Higgs C, et al. Pharmacokinetics of once-daily darunavir-ritonavir and atazanavir-ritonavir over 72 hours following drug cessation. Antimicrob Agents Chemother. 2011; 55:4218–4223. [PubMed: 21709075]
20. Kuypers DR. Immunotherapy in elderly transplant recipients: a guide to clinically significant drug interactions. Drugs Aging. 2009; 26:715–737. [PubMed: 19728747]

21. Bartlett JA, Shao JF. Successes, challenges, and limitations of current antiretroviral therapy in low-income and middle-income countries. Lancet Infect Dis. 2009; 9:637–649. [PubMed: 19778766]
22. Jain R, Clark NM, Diaz-Linares M, Grim SA. Limitations of current antiretroviral agents and opportunities for development. Curr Pharm Des. 2006; 12:1065–1074. [PubMed: 16515486]
23. Nowacek A, Kosloski LM, Gendelman HE. Neurodegenerative disorders and nanoformulated drug development. Nanomedicine (Lond). 2009; 4:541–555. [PubMed: 19572820]
24. Nowacek A, Gendelman HE. NanoART, neuroAIDS and CNS drug delivery. Nanomedicine (Lond). 2009; 4:557–574. [PubMed: 19572821]
25. Kanmogne GD, Singh S, Roy U, Liu X, McMillan J, Gorantla S, et al. Mononuclear phagocyte intercellular crosstalk facilitates transmission of cell-targeted nanoformulated antiretroviral drugs to human brain endothelial cells. Int J Nanomedicine. 2012; 7:2373–2388. [PubMed: 22661891]
26. Upal Roy JM, Alnouti Yazen, Gautam Nagsen, Smith Nathan, Balkundi Shantanu, Dash Prasanta, Gorantla Santhi, Martinez-Skinner Andrea, Meza Jane, Kanmogne Georgette, Cohen Samuel M, Mosley R Lee, Poluektova Larisa, Gendelman Howard E. Pharmacodynamic and anti-retroviral activities of combination nanoformulated antiretrovirals in HIV-1-infected human PBL-reconstituted mice. Journal of infectious Diseases. 2012 **In Press.**
27. Klotz U. Pharmacokinetics and drug metabolism in the elderly. Drug Metab Rev. 2009; 41:67–76. [PubMed: 19514965]
28. Felmlee MA, Lon HK, Gonzalez FJ, Yu AM. Cytochrome P450 expression and regulation in CYP3A4/CYP2D6 double transgenic humanized mice. Drug Metab Dispos. 2008; 36:435–441. [PubMed: 18048490]
29. Gorantla S, Gendelman HE, Poluektova LY. Can humanized mice reflect the complex pathobiology of HIV-associated neurocognitive disorders? J Neuroimmune Pharmacol. 2012; 7:352–362. [PubMed: 22222956]
30. Gorantla S, Makarov E, Finke-Dwyer J, Castanedo A, Holguin A, Gebhart CL, et al. Links between progressive HIV-1 infection of humanized mice and viral neuropathogenesis. Am J Pathol. 2010; 177:2938–2949. [PubMed: 21088215]
31. Gorantla S, Poluektova L, Gendelman HE. Rodent models for HIV-associated neurocognitive disorders. Trends Neurosci. 2012; 35:197–208. [PubMed: 22305769]
32. Chun TW, Nickle DC, Justement JS, Meyers JH, Roby G, Hallahan CW, et al. Persistence of HIV in gut-associated lymphoid tissue despite long-term antiretroviral therapy. J Infect Dis. 2008; 197:714–720. [PubMed: 18260759]
33. Choi A, Scherzer R, Bacchetti P, Tien PC, Saag MS, Gibert CL, et al. Cystatin C, albuminuria, and 5-year all-cause mortality in HIV-infected persons. Am J Kidney Dis. 2010; 56:872–882. [PubMed: 20709438]
34. Foreman O, Kavirayani AM, Griffey SM, Reader R, Shultz LD. Opportunistic bacterial infections in breeding colonies of the NSG mouse strain. Vet Pathol. 2011; 48:495–499. [PubMed: 20817888]
35. Taiwo B, Murphy RL, Katlama C. Novel antiretroviral combinations in treatment-experienced patients with HIV infection: rationale and results. Drugs. 2010; 70:1629–1642. [PubMed: 20731472]

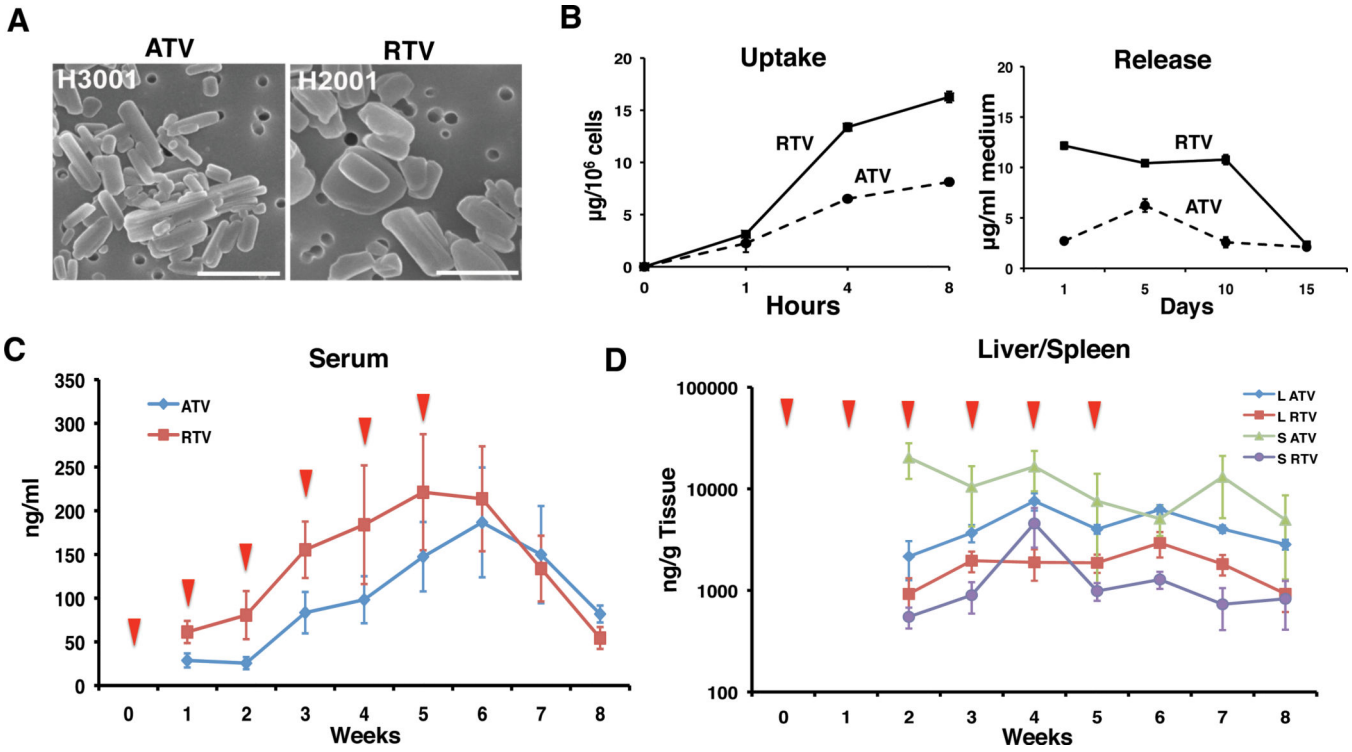

Figure 1. NanoART characterization and tissue distribution

(**A**) Scanning electron micrographs (15,000×) of nanoformulations on top of a 0.2 µm polycarbonate filter membrane are shown, bar = 1 µm. (**B**) Time course of nanoART uptake and release of monocyte-derived macrophages. Concentration in cell lysates and media were determined by RP-HPLC. Data is expressed as mean + SEM for $n = 3$ determinations. (**C**) Measurement of ATV and RTV concentrations in the serum by UPLC-MS/MS and (**D**) in liver (**L**) and spleen (**S**) ($\log_{10}$ scale) during the study time course. Uninfected 10-week old NSG mice were injected weekly subcutaneously for 6 weeks with nanoformulations of ATV and RTV (1:1) at dosages of 250 mg/kg. A group of 5 mice were sacrificed weekly and 3 weeks after drug cessation. Drug levels were quantified in sera, liver and spleen. In sera drug was detected from week-1, and in liver and spleen, drug was detected from week 2 as shown in **D**. Data are expressed as medians at the 25th and 75th percentiles for $n = 5$. Red triangles indicate nanoART injection time.

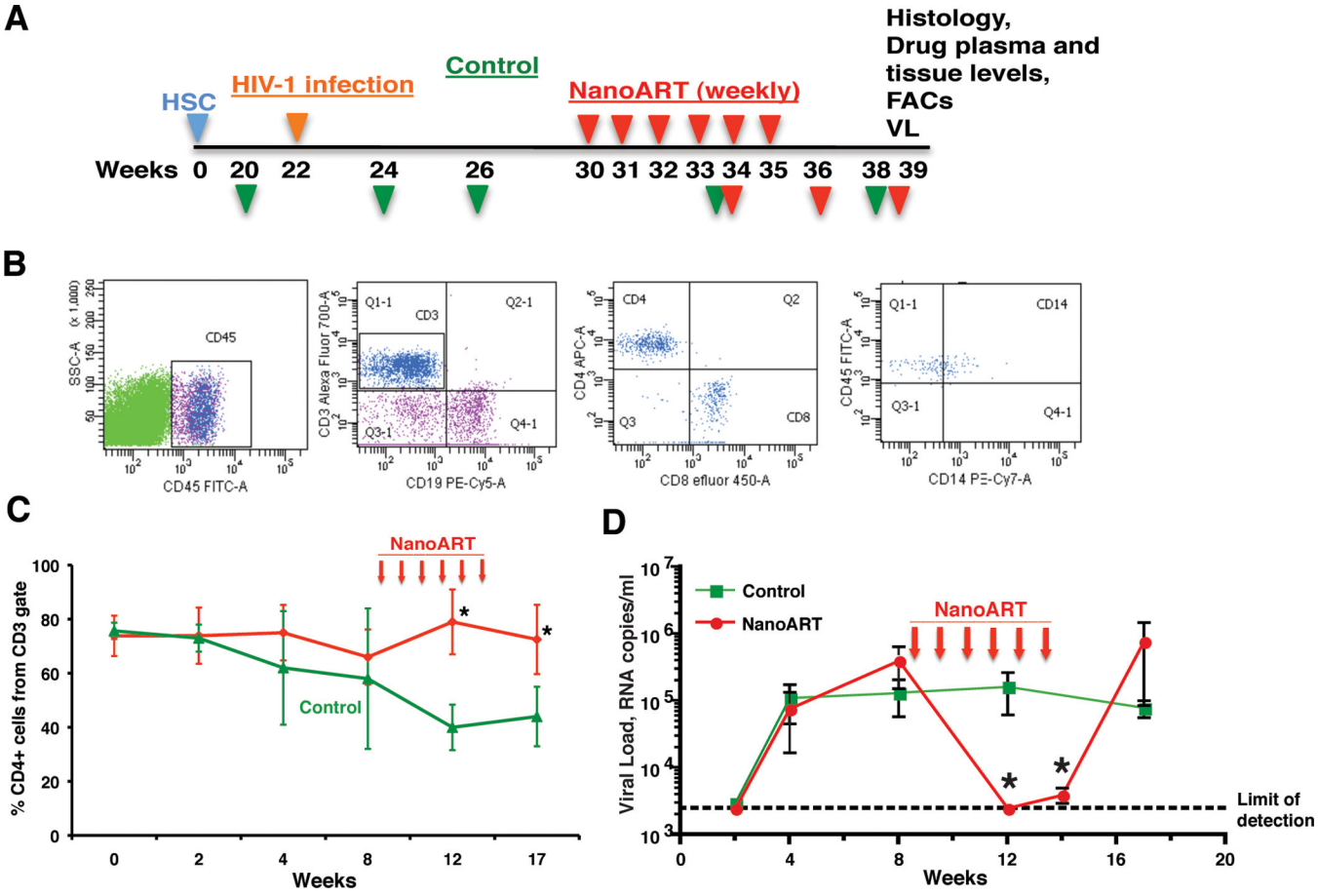

Figure 2. NanoART preserves CD4$^+$ T cells and suppresses VL

(**A**) Experimental scheme for human CD34$^+$ HSC reconstitution, HIV-1 infection, nanoART administration (above time line), and viral and immune profiling (green and red triangles below time line), drug concentration and histological evaluations are shown. (**B**) Flow cytometric plots for human cell profiles in mouse blood. Mice were bled from facial vein once every four weeks starting the second week after HIV-1 infection and peripheral blood stained for expression of human CD45. Gated human CD45+ mononuclear cells were assessed for expression of human CD3 (T cells), CD19 (B cells) and CD14 (monocytes). CD3+ T cells were gated to assess the expression of CD4 and CD8. (**C**) Circulating human CD4$^+$ T cells and **(D)** viral loads (VL) in peripheral blood during infection in untreated (control) animals and nanoART-treated mice at times (weeks) post-HIV-1 infection. VL, with rebound at 3 weeks of drug cessation and preserved CD4$^+$ T cell counts in nanoART treated animals was found. Data are expressed as mean + SEM for n = 5. *Significantly different at $p<0.05$ compared to control.

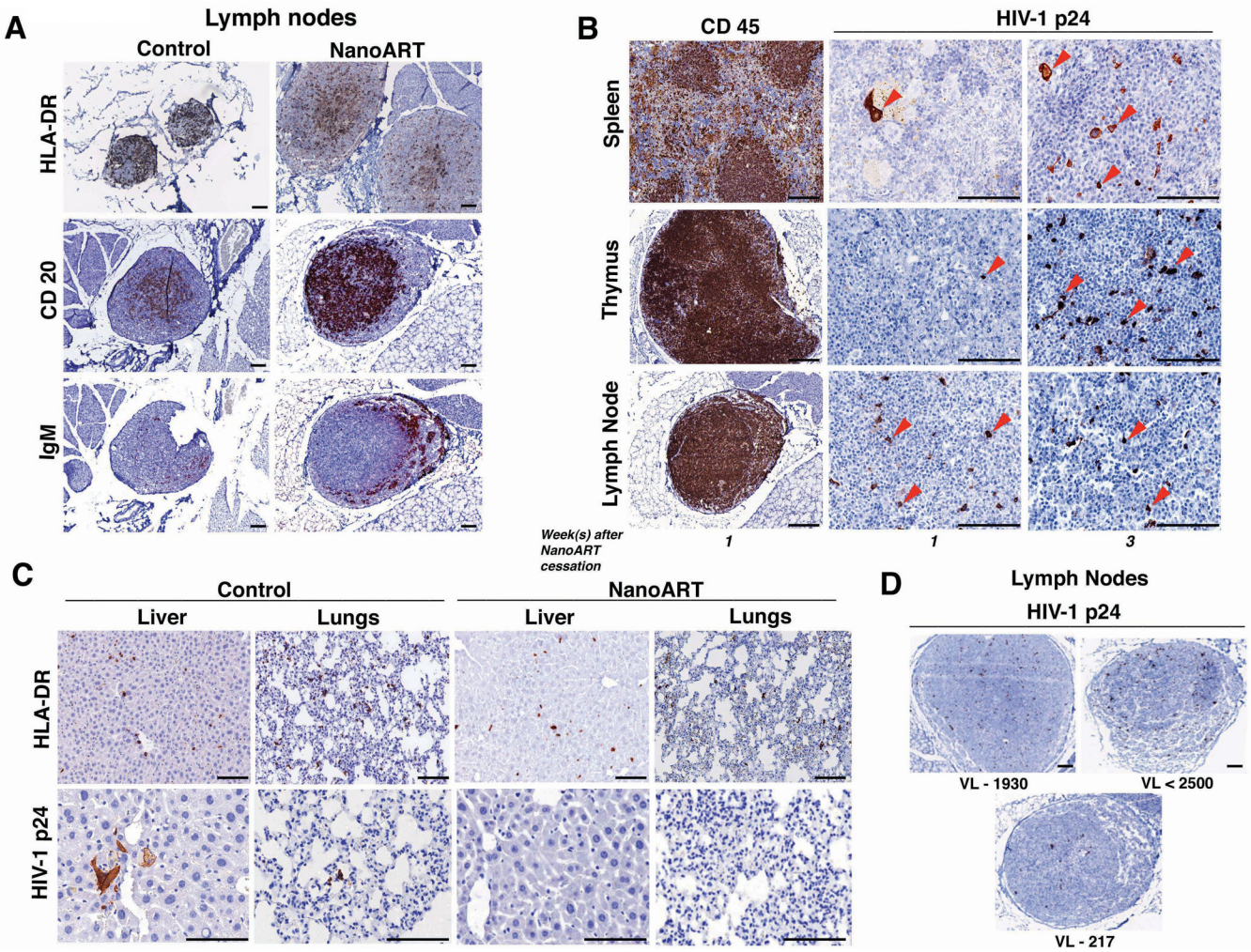

Figure 3. NanoART reduces number of infected cells and restores tissue integrity

(**A**) Histopathology of lymph nodes in HIV-1 infected humanized mice after nanoART treatment shows reductions in follicle size with evident HLA-DR and HIV-1p24+ staining. Staining of lymph nodes with anti-CD20 and anti-IgM shows the presence of mature cells in control and nanoART animals. **(B)** Histopathology of lymphoid organs of hu-NSG mice one and three weeks after cessation of nanoART. ATV and RTV nanoformulations were administered starting eight weeks after viral infection. Representative sections of spleen, thymus and lymph nodes were stained for human CD45 and HIV-1 p24 antigens (brown). HIV-1 p24+ cells, readily seen (red arrows) in splenic lymphoid follicles, thymus and lymph nodes, were affected following therapy and therapeutic interruption. **(C)** Representative liver and lung sections were stained for human HLA-DR and HIV-1 p24 in hu-NSG mice. Untreated animals showing HIV-1p24+ cells compared to nanoART treated animals. **(D)** Lymph nodes of nanoART treated mice showing numbers of HIV-1p24+ cells (brown-stained). Serum VLs are shown beneath each micrograph. The scale bar in the pictures corresponds to 100 μm.

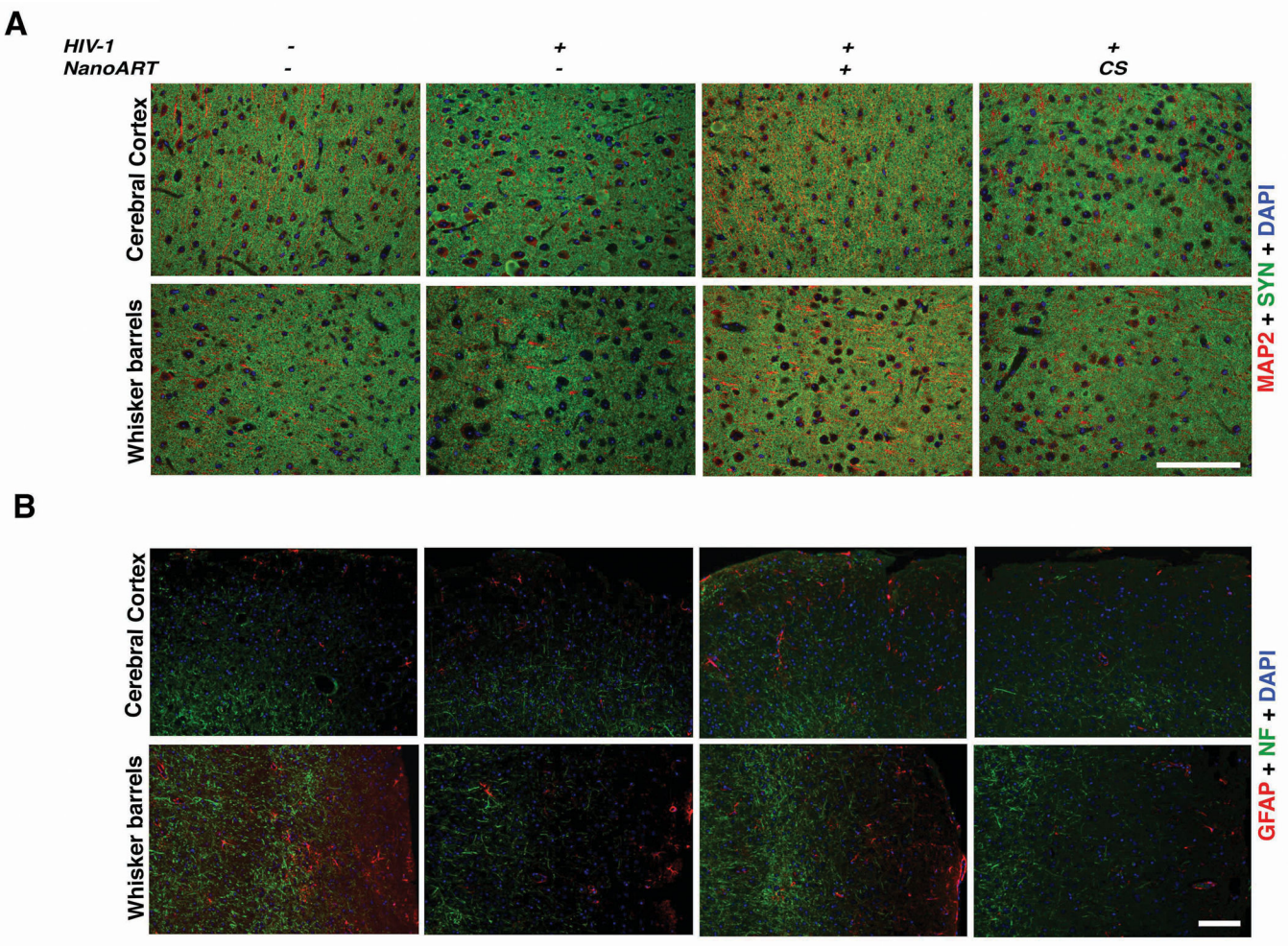

Figure 4. NanoART improves neuronal, synaptic and astrocyte markers damaged following HIV-1 infection

Immunofluorescence labeling of astrocytes, neurofilaments and synapses in brain regions of hu-NSG mice that were uninfected/untreated, infected/untreated, infected/nanoART-treated, and infected/nanoART-treated and suspended. Representative images captured with the Nuance multispectral imaging system are presented. Slide mounted sections (5 μm) of brain with VL ranging from very high (untreated and treatment interrupted group) to viral loads less than level of detection (group sacrificed 1 week after 2 nanoART injections) were stained for (**A**) dendritic MAP2, red, synaptic morphology with synaptophysin (SYN) green, and nuclei (DAPI) blue) and (**B**) GFAP, red, neurofilament (NF) green nuclei (DAPI) blue. Infected and nanoART treated groups have extended dendritic morphological appearance as compared to infected and treatment cessation group, where punctate structures were observed. The scale bar corresponds to 100 μm. CS is nanoART cessation.

AIDS. Author manuscript; available in PMC 2014 May 18.

Table 1

Individual levels of viral load (VL), human cells and drug concentration in humanized and HIV-1 infected mice.

Groups	Mouse #	Sex	Peripheral blood				Liver Drugs, ng/ml	
			VL, copies/ml	Human CD45$^+$ cells, %	Drugs in serum, ng/ml			
					ATV	RTV	ATV	RTV
HIV-1	1157	F	102000	15	NA	NA	NA	NA
	1160	M	40100	2.8	NA	NA	NA	NA
	1162	F	91000	29.8	NA	NA	NA	NA
	1172	M	4750	2.7	NA	NA	NA	NA
	1175	M	72500	33.7	NA	NA	NA	NA
	1176	F	162000	48.4	NA	NA	NA	NA
+NanoART (2 injections)[a]	1177	F	1930	9.3	488	235	1681	2220
	1174	F	217	6.4	655	231	3134	2520
+NanoART (6 injections, 3 week **treatment cessation** (CS)	1173	M	< 2500	25.9	237	40	1089	376
	1164	M	6550	20.2	227	80	492	416
	1171	M	117500	3.0	226	40	5663	296
	1187	M	221000	16.8	235	95	1264	515
	1217	M	>3550000	51.5	128	32	364	144
				Median	227	40	1089	376
Uninfected +NanoART (6 injections)	1179	F	NA	7.4	367	41	1413	690
	1180	F	NA	22.4	309	60	15592	2410
	1181	F	NA	16.1	663	106	1817	1265
	1151	M	NA	10.4	210	49	974	358
	1170	F	NA	2.0	381	54	1816	555
				Median	367	54	1816	690
				Mann-Whitney U-test[b]	0.095	0.421	0.222	0.056

[a] Mice were sacrificed 7 days after 2nd nanoART injection; all other mice were sacrificed 3 weeks post 6 (weekly) nanoART treatment. Mice 1177 (initial VL 296000) and 1174 (78500 RNA copies/ml) serum samples were tested at a lower dilution such that values obtained were lower than the detection limit. "+NanoART" at 1 and 3 weeks refer to the time the last drug injection.

[b] Comparison of drug concentrations between uninfected and HIV-1-infected mice. NA - Not Available